PERGAMON

Journal of Atmospheric and Solar-Terrestrial Physics 62 (2000) 437–447

Journal of ATMOSPHERIC AND SOLAR-TERRESTRIAL PHYSICS

Effects of various transport processes on the streaming ion density during the first stage of plasmaspheric refilling

M.W. Liemohn[a,*], J.U. Kozyra[a], G.V. Khazanov[b], P.D. Craven[c]

[a]*Space Physics Research Laboratory, University of Michigan, Ann Arbor, MI 48109, USA*
[b]*Geophysical Institute and Physics Department, University of Alaska, Fairbanks, AK 99775, USA*
[c]*Space Sciences Laboratory, Marshall Space Flight Center, Huntsville, AL 35812, USA*

Received 30 July 1999; received in revised form 5 November 1999; accepted 18 November 1999

Abstract

The dependence of the first stage H^+ plasmaspheric refilling density on various parameters is examined using a kinetic transport model. The first stage of refilling is defined as the time for the source cone to reach a quasi-steady-state level. Three influencing factors are examined in detail. The first two factors are actually studying numerical influences of physical phenomena. That is, the method of including these processes in the calculation is varied to determine the importance of calculational rigor. The two processes of interest are self-collisional feedback and the ambipolar electric field. The third influencing factor to be examined is the effect of coexistent energetic populations of the refilling rate. It is found that the results greatly depend on the method of incorporating self-collisions into the model, as the scattering and loss processes of the low-energy proton population interacting with itself has a significant influence on the early stage density. This interaction is particularly strong in the low-altitude region where the densities are high enough to substantially alter the distribution function. It is also found that the ambipolar electric field is the dominant force term, increasing the densities in the plasmasphere by accelerating the particles through the low-altitude scattering zone. The hot populations are found to have only a minor influence near the equatorial region, where they slow the H^+ streams down and cause the density to slightly increase. The effects of hot ions are more pronounced in the streaming velocity and the temperature anistropy, but still confined to the equatorial region.

Keywords: Plasmasphere; Ionosphere–magnetosphere coupling; Magnetic storms

1. Introduction

In the outer region of the plasmasphere, the cold ion populations are often not in an isotropic equilibrium state. This region is often depleted of its plasmaspheric material during geomagnetic disturbances, and subsequently refilled upon a return to quiet activity levels (e.g., Carpenter, 1966; Angerami and Carpenter, 1966; Carpenter et al., 1969). This refilling begins with ion streams from the ionospheres. These particles undergo pitch angle focusing as they move along the field lines, and thus this population has a source cone velocity space distribution function. This distribution is far from a Maxwellian (Singh, 1988), and its transition to an isotropic Maxwellian is less than fully understood.

* Corresponding author. Tel.: +1-734-647-4705; fax: +1-734-647-3083.
E-mail address: liemohn@umich.edu (M.W. Liemohn).

1364-6826/00/$ - see front matter
PII: S1364-6826(00)00018-3

Additionally, the density of this source cone population plays a crucial role in the refilling rate, as the amount of scattering into the trapped zone is dependent on the density of the scattering targets (the streaming ions themselves). It is, therefore, necessary to understand the nature of the early stages of the plasmaspheric refilling process in order to predict the development of the later stages. Of particular interest is the first stage of refilling, that is, the initial flow of particles from the ionospheres through the magnetosphere until the source cone reaches a quasi-steady-state level. The characteristics at this time define the initial long-term rate of refilling into the trapped zone.

Defining the density in the source cone is not a straightforward collisionless mapping of the ionospheric input flux along the field line. Because these particles have low energies (less than or equal to a few electron volts), they (1) readily scatter with themselves and other particles, (2) are influenced by even the slightest parallel electric fields, and (3) can interact with low-frequency plasma waves. The effects of these processes on plasmaspheric refilling have been examined in many modeling efforts (see reviews by Singh and Horwitz, 1992; Singh et al., 1994; Carpenter and Lemaire, 1997), but conclusive determinations of some issues are still unresolved.

For instance, plasmaspheric refilling often manifests itself in the midst of numerous other plasma constituents populating the inner magnetosphere. These other populations include the remnants of the previous cold isotropic plasmasphere, parallel-streaming superthermal electrons, warm highly-anisotropic ion populations, energetic ring current ions, and relativistic electrons (see Sojka et al., 1983). These other populations can play a vital role in determining the density of the source cone and the rate at which these particles are scattered into the depleted trapped zone. The role of these other coexistent plasma populations on the plasmaspheric refilling rates is unclear, especially their influence on the initial refilling rates into the depleted trapped zone.

This study expands on the recent study of Liemohn et al. (1999) by investigating the relationship of various effects on the early stages of plasmaspheric refilling. Here, the focus is on the first 90 min of refilling (the initial stage of refilling for H^+ ions along an $L = 4$ field line). This will be done by simulating the flow of H^+ along a chosen field line with a kinetic transport model. Several input parameters, background population characteristics, and interaction terms will be manipulated to investigate their influence on the refilling process. In particular, three things will be altered: (1) the temperature used in the collision term for the cold H^+ self-interactions; (2) the field-aligned force term; and (3) the density of coexistent energetic particles.

2. Model

The model to be used in this study was initially developed for superthermal electron transport in the ionosphere and plasmasphere (along a single flux tube) to investigate the refilling and depletion timescales for that population (Khazanov et al., 1993). It solves the time-dependent, gyration-averaged kinetic equation for a plasma species' phase–space density distribution f (t, s, E, μ_0) as a function of time t, field-aligned distance s, energy E, and cosine of the equatorial pitch angle μ_0 (Khazanov et al., 1993; Liemohn et al., 1997),

$$\frac{\beta}{\sqrt{E}}\frac{\partial f}{\partial t} + \mu\frac{\partial f}{\partial s} + \frac{1-\mu^2}{2}\frac{F}{E}\frac{\partial f}{\partial \mu_0} + F\mu\frac{\partial f}{\partial E} = Q + S_{\text{coll}} \quad (1)$$

where $\beta = \sqrt{m/2} = 7.19 \times 10^{-7}$ $\text{eV}^{1/2}$ s/cm for H^+, with m being proton mass; $F_\parallel$ includes all parallel forces acting on the plasma species, particularly the field-aligned electric field (in units of eV/cm); Q is the source term; and S_{coll} represents the collisional terms. Note that magnetic mirroring is included in this formulation by the use of equatorial pitch angle as a velocity variable. In the s–μ_0 plane, particles travel along lines of constant μ_0 (conserving the first adiabatic invariant). When the mirror point for a given μ_0 is reached, that is, when $\mu = 0$, then

$$\mu_0 = \mu_{0,\,\text{m}} = \sqrt{1 - \frac{B_0}{B(s)}} \quad (2)$$

At this spatial location, $f(\mu_0)$ is moved to $-\mu_{0,\,\text{m}}$ and the particles proceed in the opposite direction along the field line. Of course, this collisionless bounce motion is violated by the processes of electric field interactions and collisions, but these are relatively slow compared to motion along the field line, and thus this transformation is advantageous because numerical diffusion is greatly reduced. Please see Khazanov et al. (1993) and Liemohn et al. (1997) for further details of this transformation.

Because the low-altitude boundary is chosen to be above the thermosphere (at 1000 km), atmospheric interactions can be neglected. The collision term can then be written as (Shkarofsky et al., 1966; Khazanov et al., 1994)

$$\begin{aligned} S_{\text{coll}} &= S_{\text{Coulomb}} \\ &= A\sum_\alpha n_\alpha \left\{ \frac{2}{E}\frac{\partial}{\partial E}\left[\frac{G_\alpha E f}{T_\alpha} + G_\alpha E\frac{\partial f}{\partial E}\right] \right. \\ &\quad \left. + \frac{\Phi_\alpha - G_\alpha}{4E^2}\frac{B_0\mu}{B\mu_0}\frac{\partial}{\partial \mu_0}\left[\frac{\mu}{\mu_0}\left(1-\mu_0^2\right)\frac{\partial f}{\partial \mu_0}\right]\right\} \end{aligned} \quad (3)$$

where n_α is the density of background species α, Φ_α is

the error function with argument $x = v/u_{\alpha t}$, with $u_{\alpha t} = (k_B T_\alpha / m_\alpha)^{1/2}$ being the thermal speed of species α; and G_α has the same argument and is defined as

$$G_\alpha = G(x) = \frac{\Phi(x)}{2x^2} - \frac{\exp(-x^2)}{x\sqrt{\pi}}$$

Note that the sum over plasma species includes the ion population being calculated by the kinetic equation (H^+). The values for this species will be either chosen and held fixed for the simulation or calculated from the results of the previous time step (to be discussed below). In this way, Eq. (3) is still linear, but can include self-consistent collisional processes. Both the pitch angle and the energy diffusion operators are included in the calculation.

Of interest in this study is the dependence of the H^+ refilling rate on the self-collisional interaction terms. That is, one of the species being summed in Eq. (3) is the ionospheric H^+ being calculated by Eq. (1). A rigorous approach involves calculating the density and temperature of these particles along the field line at each time step and using these values in Eq. (3) for the next time step. However, a simpler option will also be used to examine the level of computational effort needed to accurately determine the influence of this term. Specifically, a constant value for T_{H^+} will be used in Eq. (3) for some of the calculations, regardless of what the solution of Eq. (1) yields. Another method will calculate a single temperature from the results of Eq. (1) for use in Eq. (3). Still another approach to be used is the calculation of two temperatures from the solution of Eq. (1), one for each ion stream (split at $\mu = 0$).

Investigation of the influence of the force term is also of interest in this study. Therefore, inclusion of this term will vary depending on the simulation. Some will have this quantity fixed at zero, while some will self-consistently include it along the field line. Self-consistent inclusion of F means determining F from the solution at the previous time step using the electron momentum equation, which is dominated by the thermal electron pressure gradient (see, for example, Eq. (9) in Liemohn et al. (1997)). This pressure gradient is calculated from the spatial profile of the thermal electron density, flux, and temperature. The thermal electron density and flux are defined to balance the total ion values (using the quasi-neutrality and currentless assumptions), and the thermal electron temperature is calculated from the electron energy equation (see, for example, Eq. (27) in Khazanov et al. (1997)).

The kinetic equation is solved by replacing the derivatives with a combination of first and second order discrete differences and advancing the solution on a predefined grid in phase space. It uses a time-splitting technique to solve each derivative separately. The independent variable domains are as follows: field-line distance from 1000 km altitude up along a symmetric $L = 4$ dipole field line to 1000 km altitude in the conjugate ionosphere; energies from 0.025 up to 12 eV; and μ_0 from -1 to 1. Note that there is a region in the s–μ_0 plane that is inaccessible. This is the range from $-\mu_{0,\,m}$ to $\mu_{0,\,m}$ defined in Eq. (2). No local pitch angles are left out of the calculation, however, because this gap is from the transformation from μ to μ_0, and the inner edges of the μ_0 region of existence are where $\mu = 0$. The values of f on each side of this gap are identical.

An input H^+ phase space density from the ionosphere is prescribed, defined as a Maxwellian with density 2×10^3 cm^{-3} and temperature 0.3 eV. However, the downward flux at the boundaries are calculated by the model, yielding a variable net flux across the boundary on the order of 10^8 cm^{-2} s^{-1} (typically 1–2 times of this). A thermal oxygen ion population was imposed along the field line, with a density ranging from 8×10^3 cm^{-3} at the lower boundary to 0.2 cm^{-3} at the equatorial plane, held constant with time. This time-independence assumption is valid because of the much longer refilling timescale of O^+ compared to the simulation length (90 min).

For several of the simulations, hot, trapped plasma populations are imposed by defining an equatorial plane density and using

$$n(s) = \frac{n_0 B_0 (B_1 - B(s))}{\left[AB(s) - B_0(A-1)\right](B_1 - B_0)} \tag{4}$$

to map it along the field line (cf., Lemaire and Scherer, 1971; Liemohn and Khazanov, 1998). This density is independent of the field-aligned potential because the characteristic energies of these populations are much greater than the potential drop, so these terms were omitted. In Eq. (4), $A = T_\perp / T_\parallel$ of the hot population at the equator and is assigned, and the subscript "1" denotes values at the lower altitude boundary. Note that this density mapping is equal to the assumed n_0 at the equatorial plane, is equal to zero at the ionospheric boundary, and imposes no net flux for the hot population. These values are included in the scattering operators and in the quasineutrality condition (thus, contributing to the electric field).

For comparison with the calculated results, the low-altitude boundary condition will also be mapped along the field line. In the absence of collisions and nonmagnetic field-aligned forces, the only process acting on the particles is pitch angle focusing due to the inhomogeneous geomagnetic field. Thus, the density along the field line (taking into account both source regions) is given by (Liemohn and Khazanov, 1998).

Table 1
Simulation characteristics and equatorial plane densities at 90 min

Simulation scenario	T_{H^+}scat used in Eq. (3)	F used in Eq. (1)	Included hot populations	Density n_{H^+}, eq (90 min)
1	$\equiv 0.5$ eV	$\equiv 0$	None	8.2 cm^{-3}
2	$\equiv 0.3$ eV	$\equiv 0$	None	5.9 cm^{-3}
3	$\equiv 0.05$ eV	$\equiv 0$	None	2.5 cm^{-3}
4	Single fit from prev. Δt	$\equiv 0$	None	3.7 cm^{-3}
5	Double fit from prev. Δt	$\equiv 0$	None	4.5 cm^{-3}
6	Single fit from prev. Δt	From prev. Δt	None	9.0 cm^{-3}
7	$\equiv 0.3$ eV	From prev. Δt	None	11.52 cm^{-3}
8	Single fit from prev. Δt	From prev. Δt	Case 1	9.6 cm^{-3}
9	Single fit from prev. Δt	From prev. Δt	Case 2	10.6 cm^{-3}
10	Single fit from prev. Δt	From prev. Δt	Case 3	11.6 cm^{-3}
Density from Eq. (5)	–	–	–	13.7 cm^{-3}

$$n(s) = n_1\left(1 - \sqrt{1 - \frac{B(s)}{B_1}}\right) \tag{5}$$

Because it is collisionless, this distribution has no particles outside of the source cone in velocity space, that is, the trapped zone is empty. This density profile will be discussed in greater detail in the following section.

3. Results and discussion

Simulations were conducted to investigate the effects of various transport processes on the H^+ density during the first stage of plasmaspheric refilling. Table 1 lists the characteristics of the various simulation scenarios presented in this section.

The first issue to be examined is the influence of the H^+ temperature on the source cone density. Note that this is an investigation of the numerical effect of the value of this physical quantity. That is, self-collisions are known to occur, but their significance on the early stage refilling rate is debatable. If the influence is minor, then it may be desireable to choose a simple approach for including this nonlinear process. Conversely, if the influence is major, then a sophisticated approach is essential. Therefore, this study will examine the level of computational rigor necessary to obtain a reasonable result.

Initially, the model is run with a given background H^+ temperature in the collision operator (3). Note that the temperature of the injected H^+ ions is kept at 0.3 eV; only the T_{H^+} in the scattering term is altered. Also in these results, the field-aligned force term F in Eq. (1) is set to zero everywhere (magnetic focusing and mirroring is still included). This is done to isolate the influence from the scattering term temperature. While this is clearly not a self-consistent solution, it will nonetheless help to quantify the effect of this term.

Fig. 1 shows the field-line density distribution after 90 min for three simulations with different scattering population temperatures: 0.5, 0.3, and 0.05 eV. Also plotted is the density computed from Eq. (5). It is seen that as this background temperature increases, so does the calculated plasmaspheric density. The values of these densities at the equatorial plane after 90 min are given in Table 1. This indicates that the self-collisional H^+ scattering is very important in defining the early stage density. In the low-altitude regions, it is seen that the 0.3 and 0.5 eV curves are higher than the density from Eq. (5), a result of material rapidly scattering into the trapped zone at these altitudes. At higher altitudes, though, all of the simulated results are below the density from Eq. (5) because the low-energy source cone has been depleted compared to the collisionless mapping.

To better illustrate this, Fig. 2 shows pitch angle distributions at the equatorial plane after 90 min at several energies for the four results of Fig. 1. The source

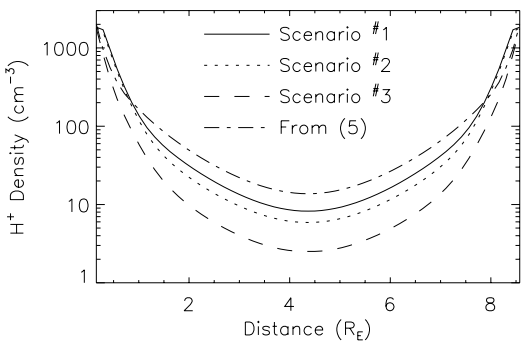

Fig. 1. Refilling densities after 90 min for three cases of given background T_H^+ values used in Eq. (3), as well as the density profile from Eq. (5). See Table 1 for simulation scenario descriptions.

cone boundary is marked by the edge of the collisionlessly-mapped distribution (dash–dotted line). It is clear that substantial scattering and loss occurred at low energies and the higher energies maintained more of their source cone populations. This is due to the large amount of pitch angle scattering occurring at low altitudes, depleting the low-energy range of the flux function more so than the high-energy range. This scattering causes particles to move from the source cone through the trapped zone and into the other source cone (now a loss cone, because the particles will travel back down the field line and out of the simulation domain). At the equatorial plane, the low-energy distributions are already approaching isotropy, while the higher energy particles are still quite far from such a state. This was also found for superthermal electrons in the plasmaspheric trapped zone by Khazanov et al. (1993) and Khazanov and Liemohn (1995). The kink in the higher-energy distributions in the 30–50° region is the remnants of the initial condition distribution showing up in the results. The initial condition was chosen to be quite a bit lower than the injected distribution to minimize this effect, yet large enough to still be realistic for the simulations. It is also interesting to see that the 0.3 eV curve is close to the 0.5 eV curve for low energies, but then is closer to the 0.05 eV curve at higher energies. This is from the energy and scattering temperature dependence in Eq. (3), which affects not only the energy losses but also the pitch angle scattering through the Φ and G coefficients.

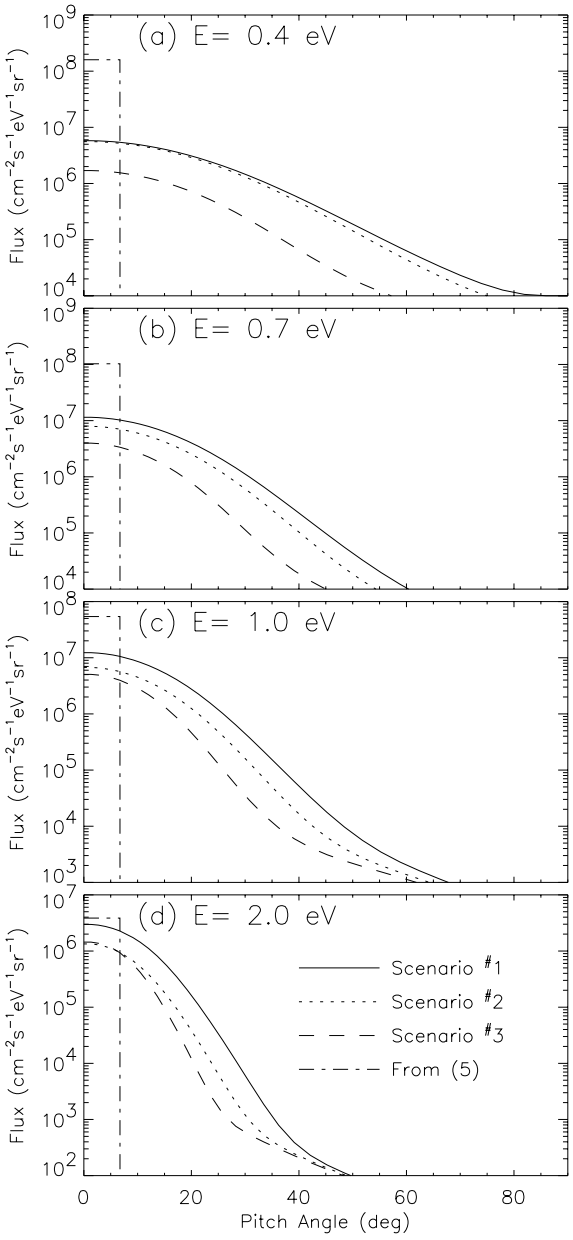

Fig. 2. Equatorial pitch angle distributions at several energies for the results shown in Fig. 1 (also at 90 min).

Another series of simulations were conducted to examine the influence of a self-consistently-calculated temperature in the scattering term. Fig. 3 shows results from these calculations, plotting density after 90 min for several runs. Two of the results were shown in Fig. 1: the density with a 0.3 eV imposed background temperature; and the density from Eq. (5). The other two results are from self-consistent calculations: one with a single density and mean energy determined from the previous time step and used as background parameters in the collision operator; and the other with two sets of moments taken from the previous time step (one for $\mu > 0$ and another for $\mu < 0$) and used as two separate background populations in Eq. (3). In the following discussion, these two results will

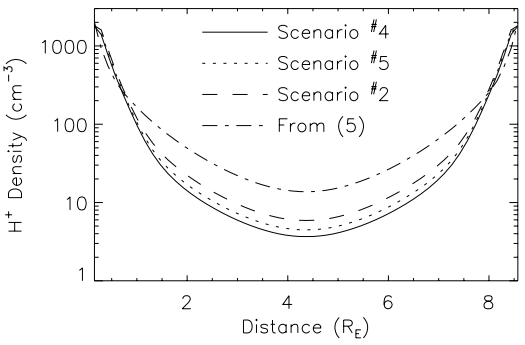

Fig. 3. Density profiles after 90 min for simulations with T_{H^+} in Eq. (3) taken from the previous time step results, as well as a given T_{H^+} case and the results from Eq. (5). See Table 1 for simulation scenario descriptions.

be referred to as the single moment and double moment self-consistent result sets, respectively. Comparing these two self-consistent methods is useful because a single temperature value integrated over both streams overestimates the actual temperature of each individual stream. Therefore, this is another test of the level of rigor needed to accurately incorporate this term. It is seen that the amount of material along the field line is smallest for the single moment set results, and that the double moment set results have 20% more protons at the equator than the single moment results (see Table 1). This again illustrates the importance of self-collisions in the development of the low-energy H^+ distribution, and that the choice of feedback method matters. Here are two self-consistent results with different feedback methods yielding different results.

It is interesting that both of these results are less than the results that used an imposed constant background temperature. This can be explained by examining the background temperature profiles from these simulations (that is, the temperature used in Eq. (3)). These temperature profiles are plotted in Fig. 4 for the three simulations at a time 90 min into the simulation. Note that while the self-consistently calculated background temperatures are higher than the imposed temperature for most of the field line, they are much lower than the imposed value near the ionospheres. Because this is the region of highest density, far more scattering occurs in these low-altitude regions, and so these temperatures play a larger role in determining the loss rate. Also, the local pitch angle extent of the trapped zone is smaller near the ionosphere compared to near the equator. This means that particles have less $\Delta\mu_0$ to scatter through to turn around and re-enter the ionosphere. As noted in the first set of simulations, lower background temperatures lead to more scattering and loss. This emphasizes the fact that it is the low-altitude region that predominantly determines the early stage density profile.

Another factor that influences this early stage density is the presence of a parallel force term. While this term includes gravity and the ambipolar electric field, the dominant term in F is the thermal electron pressure gradient. Thus it is directed upwards for H^+ (not necessarily for O^+, for which the gravitational potential is much larger), accelerating the streams towards the equatorial plane and then decelerating them as they continue towards the conjugate ionosphere. As with the temperature investigations above, this is an examination of the numerical effects from different levels of calculational rigor.

Because the electron density and temperature are time dependent, the force term is calculated self-consistently by using the pressure from the previous time step. Results of two simulations with F included are shown in Fig. 5, along with the density profiles from the corresponding simulations with $F \equiv 0$ and the density from Eq. (5). These two sets of runs are for with and without a self-consistently-calculated background H^+ temperature. The influence of the electric field is clearly seen in this plot; the densities are greatly enhanced, double the values at the equatorial plane over those without a force term (see Table 1). Examining the spatial profiles of these results indicates that the ambipolar electric field is strongest near the ionosphere. This causes the ions to move faster through the collisional region near the lower boundaries, and thus more particles remain in the stream.

Finally, the influence of equatorially trapped populations on the rate of early stage refilling is investigated. Because feedback effects are important for this interaction, all self-consistent processes are included in

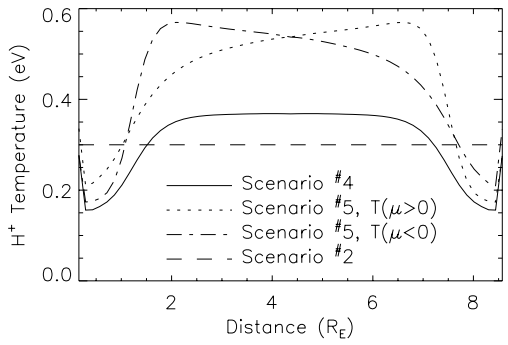

Fig. 4. Spatial profiles of the scattering temperatures used in Eq. (3) for the results shown in Fig. 3 (also at 90 min).

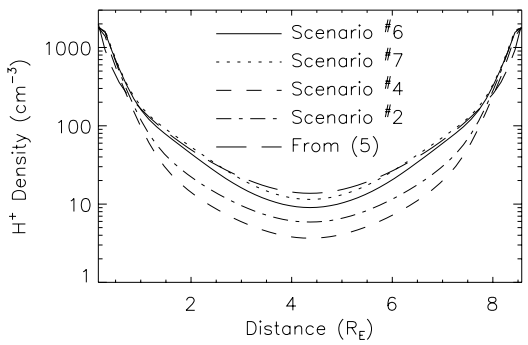

Fig. 5. Density profiles after 90 min for simulations with the parallel force term F included and taken from the previous time step (scattering T given and calculated), as well as corresponding results without F and the results from Eq. (5). See Table 1 for simulation scenario descriptions.

Table 2
Hot population characteristics

m/m_p	n_0 (cm^{-3})	$T_\perp$ (eV)	$T_\perp/T_\parallel$	Description
Case 1: moderate ring current (RC)				
1	0.5	5000	5	Low-E RC H^+
1	1.0	50,000	5	High-E RC H^+
16	3.0	5000	5	Low-E RC O^+
16	2.5	50,000	5	High-E RC O^+
Case 2: strong RC				
1	1.0	5000	5	Low-E RC H^+
1	4.0	50,000	5	High-E RC H^+
16	10.0	5000	5	Low-E RC O^+
16	10.0	50,000	5	High-E RC O^+
Case 3: strong RC with warm pancake ions				
1	10.0	5000	5	Low-E RC H^+
1	4.0	50,000	5	High-E RC H^+
16	10.0	5000	5	Low-E RC O^+
16	10.0	50,000	5	High-E RC O^+
1	20.0	25	20	Pancake H^+

this set of simulations. The three cases for the hot population equatorial values are listed in Table 2, with the three sets representing typical values of a moderate storm-time ring current, a very strong ring current, and a very strong ring current with an additional warm "pancake" distribution (Olsen et al., 1994; Kozyra et al., 1998). One would expect the presence of an equatorially confined ion population to create an electrostatic barrier to prevent other ions from reaching this region. Therefore, these hot populations should hinder the cold ion streams from reaching the conjugate ionosphere. Fig. 6 shows density profiles after 90 min from these three simulations, from the fully self-consistent simulation without a hot population, and from Eq. (5). Rather than seeing a decrease in density due to the presence of hot populations, an increase in cold ion density with increasing hot ion density is found (see also Table 1). This can be explained by examining the field-line profiles of the potential (integrated force term). Fig. 7 presents these potential profiles (after 90 min) for the simulations. Just as expected, there is a barrier near the equator that increases with hot ion density, but it is not enough to overcome the potential drop at lower altitudes and thus the outflowing streams still penetrate through to the conjugate ionosphere. The influence of these potential barriers is seen in Fig. 6 as a plateau in density in the equatorial region. This is due to the slowing of the streaming ions, causing a build up coincident with the barrier (pile-up effect). In fact, the low-altitude density profiles are all quite similar, and the influence of the hot populations does not reach much beyond the equator. This is largely due to the greater density of streaming particles compared to the hot populations away from the equator, and the energetic particles are simply overwhelmed. It could be conceived, however, that if the influence of the hot particles on the electric field was increased to the point of creating a barrier larger than the low-altitude drop, then a dramatic change would occur in the cold ion density as they would no longer increase but instead decrease rapidly with hot ion density (as originally predicted).

This potential barrier also has an effect on the calculated temperature of the streaming protons. Fig. 8 shows temperature anisotropy ratios ($T_\parallel/T_\perp$) for the same simulations presented in Figs. 6 and 7. First, consider the upper panel, where the integrals were taken over all μ, thus including both streams in this calculation. The ratio is very high near the equator, with a maximum value over 40 when no hot ion populations are present (Scenario 6). Note that because the drift speeds of the streams are substantially larger than the

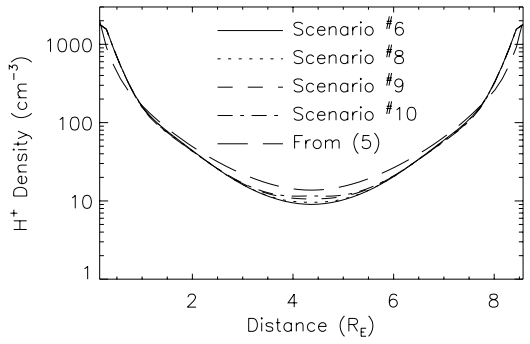

Fig. 6. Density profiles after 90 min for simulations with hot populations included (T and F calculated), along with results with a hot population and from Eq. (5). See Tables 1 and 2 for simulation scenario descriptions and hot population cases, respectively.

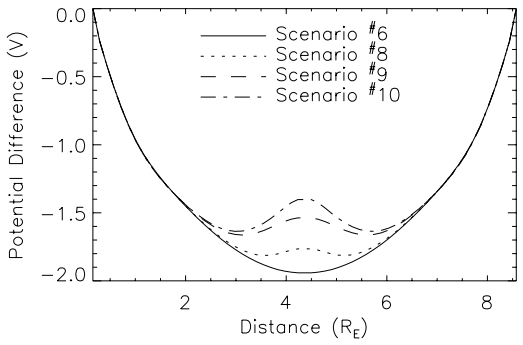

Fig. 7. Potential energy difference profiles after 90 min for the results shown in Fig. 6.

thermal velocities, the $T_\parallel$ value used in Fig. 8 (a) is really a measure of the differential speed rather than the thermal spread of the streams. The presence of the hot ions slows the streams, decreasing $T_\parallel$. In fact, this anisotropy value drops below 20 for Scenario 10 at the equatorial plane. However, this is still a large value. To understand the influence on the spread of the individual ion streams, Fig. 8 (b) shows the same ratio but for an integral over only $\mu > 0$. The footpoint values of 0.5 are expected because the streaming velocity is less than the thermal velocity at these values and the integration limit of $\mu > 0$ does not capture the true value of $T_\parallel$ at these altitudes. This is also the reason for the bump near the conjugate ionospheric interface. Near the equatorial plane, however, the plotted value better depicts the single stream temperature anisotropy (compared with Fig. 8 (a)) because of this integration limit. The peak at the equator in the Scenario 6 results is expected due to the electric and magnetic field effects on the velocity space distribution. An interesting result is seen just prior to the equatorial plane crossing; the anisotropy ratio increases due to the presence of the hot ion populations. This is because the deceleration from the potential barrier causes a spreading of the stream in the parallel direction in velocity space. The barrier reduces the parallel kinetic energy of each particle by an equal amount, but this has an unequal effect on the particles' parallel velocities, reducing $v_\parallel$ more for the lower-energy protons than for the higher-energy ones.

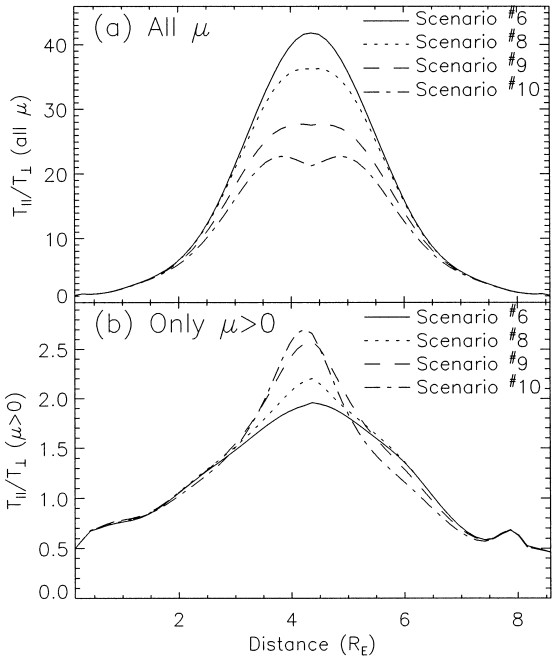

Fig. 8. H^+ temperature anisotropy ratios ($T_\parallel/T_\perp$) after 90 min for the results shown in Fig. 6. The integrals used in determining the temperature values were taken (a) over all μ values and (b) only over $\mu > 0$ (one of the streams).

To better understand these density variations, the velocity space flux spectra in the equatorial plane are shown for all of the simulations discussed above in Fig. 9. Note that only half of the distribution is shown (0–90°), and that the colorscale bar has a logarithmic scale. The basic shape of the velocity space distribution is similar in all 10 plots, although the magnitude of the number flux varies widely. In each of the plots, the lowest energies (below 0.5 eV) are already approaching isotropy, while ions well above the energy of the flux peak are barely scattered beyond the source cone. The energization in the plots on the right hand column is quite clear, shifting the flux peak in energy from less than 1 eV (Fig. 9 (b, d, and e)) up to 2 eV (Fig. 9 (f)). This peak location shifts back down slightly for the cases with hot ions present (Fig. 9 (h–j)) due to the small potential barrier at the equator (as seen in Fig. 7).

It is interesting to note the similarities and differences of these results with other computational studies of plasmaspheric refilling. For instance, both Lin et al. (1992, 1994) and Singh (1996, 1998) included thermal ion heating via wave–particle interactions in their calculations of the early stage of plasmaspheric refilling. This is a process omitted from the present study. Lin et al. (1994) demonstrated the dramatic influence of this energization term on the counterstreaming ions, particularly that a warm anisotropic ion population can be created out of the ionospheric plasma from intense wave-induced perpendicular heating. Also, the streams no longer interpenetrate but are reflected, leaving no field-aligned flows at the equator. The waves were externally imposed, however, and the heating was allowed to continue throughout the early stages of the refilling process. In contrast, the self-consistent calculations of Singh (1996, 1998) showed that heating from waves driven by the beam instability is best described as pitch angle scattering rather than perpendicular energization, and that it is quite short-lived, lasting only a few cyclotron periods ($\tau_{ci} \approx 0.1$–1 s in this region). This wave growth and decay results in a small isotropic population. He found that the ionospheric streams still interpenetrate, and in fact dominate over the density of the created trapped population. Therefore, the significance of the wave–particle interactions depends on whether or not the waves are internally or externally generated. Based on the Singh (1996, 1998) results, our assumption of neglecting the wave interactions is valid, and their inclusion should not significantly alter the main results of this study. An inclusion of a wave source such as that used in the Lin et al. (1992, 1994) studies will surely alter these results, and so the present study is limited to those times when

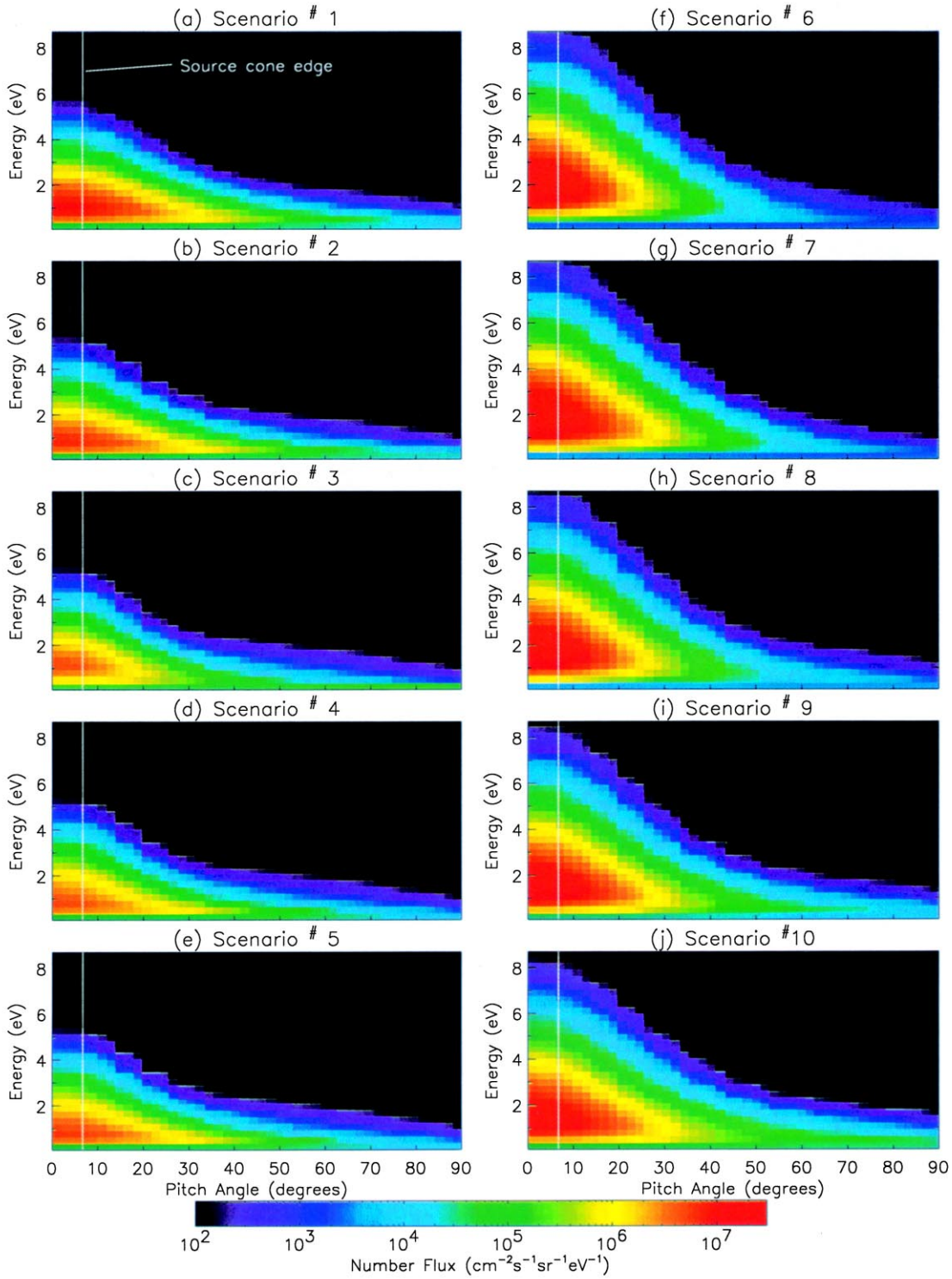

Fig. 9. Energy-pitch angle number flux spectra at the equatorial plane after 90 min for the 10 simulations discussed in the text (and listed in Table 1). The source cone pitch angle is shown as a vertical white line in each plot.

such waves are not present. As was shown by Jordanova et al. (1997), however, low-frequency waves generated by the injected plasma sheet ions are confined to the overlap region between the energetic tail particles and the plasmasphere. Therefore, this source of intense plasma waves is thought to be infrequent in the refilling zone, located beyond the plasmapause.

4. Summary

It has been shown that the H^+ density after the first stage of plasmaspheric refilling depends on many processes, and that the intensity of the controlling factors can greatly alter the amount of cold plasma along a refilling field line. From these simulations, it was seen that the simulation results strongly depend on the method of including self-collisions into the calculation. It is therefore recommended that the most sophisticated approach possible should be taken for this interaction. It was also seen that the parallel force term increases the source cone density by up to a factor of two, and should not be disregarded. In addition, the inclusion of hot populations increases rather than decreases the early stage cold ion density because the potential barrier created by their presence is insufficient to overcome the potential drop in the low-altitude region. Furthermore, it was seen that the equatorial source cone density is never as large as the collisionless mapping of the ionospheric boundary condition along the field line after 90 min of refilling. This is a result of low-altitude backscattering, and the influence of the various processes on the amount of backscattering was determined.

There are still issues to investigate in the early stages of plasmaspheric refilling. One issue is that Eq. (3) was derived assuming the background population moments are Maxwellian parameters. Examination of the velocity space distributions shown above indicates that better feedback methods are possible, and it has been noted that the choice of feedback mechanism is critical. Another issue is the procedure used to couple the hot and cold populations. More rigorous methods exist for self-consistently coupling these populations along the field line (e.g., Liemohn and Khazanov, 1998; Khazanov et al., 1998). Improved coupling procedures may result in the simulations predicting either more or less cold plasma along the field line because of the sensitivity of these ionospheric particles to the electric field. These topics will be addressed in a later study.

Acknowledgements

This work was funded by NASA grants NAG5-4771 and NAG5-6976, NSF grants ATM-9711381, ATM-9710326, and ATM-9800830, and a Research Seed Grant from the Michigan Space Grant Consortium. Also, Dr. Liemohn held a National Research Council Postdoctoral Resident Research Associateship at NASA Marshall Space Flight Center while part of this work was performed.

References

Angerami, J.J., Carpenter, D.L., 1966. Whistler studies of the plasmapause in the magnetosphere, 2, electron density and the total tube electron content near the knee in the magnetospheric ionization. Journal of Geophysical Research 71, 711–725.

Carpenter, D.L., 1966. Whistler studies of the plasmapause in the magnetosphere, 1, temporal variations in the position of the knee and some evidence of plasma motions near the knee. Journal of Geophysical Research 71, 693–709.

Carpenter, D.L., Lemaire, J., 1997. Erosion and recovery of the plasmasphere in the plasmapause region. Space Science Reviews 80, 153–179.

Carpenter, D.L., Park, C.G., Taylor Jr, H.A., Brinton, H.C., 1969. Multi-experiment detection of the plasmapause from Ogo satellites and Antarctic ground stations. Journal of Geophysical Research 74, 1837–1847.

Jordanova, V.K., Kozyra, J.U., Nagy, A.F., Khazanov, G.V., 1997. Kinetic model of the ring current–atmosphere interactions. Journal of Geophysical Research 102, 14279–14291.

Khazanov, G.V., Liemohn, M.W., 1995. Non-steady-state ionosphere–plasmasphere coupling of superthermal electrons. Journal of Geophysical Research 100, 9669–9681.

Khazanov, G.V., Liemohn, M.W., Gombosi, M.W., Nagy, A.F., 1993. Non-steady-state transport of superthermal electrons in the plasmasphere. Geophysical Research Letters 20, 2821–2824.

Khazanov, G.V., Neubert, T., Gefan, G.D., 1994. A unified theory of ionosphere–plasmasphere transport of suprathermal electrons. IEEE Transactions on Plasma Science 22, 187–198.

Khazanov, G.V., Liemohn, M.W., Moore, T.E., 1997. Photoelectron effects on the self-consistent potential in the collisionless polar wind. Journal of Geophysical Research 102, 7509–7521.

Khazanov, G.V., Liemohn, M.W., Krivorutsky, E.N., Moore, T.E., 1998. Generalized kinetic description of a plasma in an arbitrary field-aligned potential energy structure. Journal of Geophysical Research 103, 6871–6889.

Kozyra, J.U., Fok, M.-C., Sanchez, E.R., Evans, D.S., Hamilton, D.C., Nagy, A.F., 1998. The role of precipitation losses in producing the rapid early recovery phase of the Great Magnetic Storm of February 1986. Journal of Geophysical Research 103, 6801–6814.

Lemaire, J., Scherer, M., 1971. Simple model for an ion-exosphere in an open magnetic field. Physics of Fluids 14, 1683–1694.

Liemohn, M.W., Khazanov, G.V., 1998. Collisionless plasma

modeling in an arbitrary potential energy distribution. Physics of Plasmas 5, 580–590.

Liemohn, M.W., Khazanov, G.V., Moore, T.E., Guiter, S.M., 1997. Self-consistent superthermal electron effects on plasmaspheric refilling. Journal of Geophysical Research 102, 7523–7536.

Liemohn, M.W., Khazanov, G.V., Craven, P.D., Kozyra, J.U., 1999. Nonlinear kinetic modeling of early stage plasmaspheric refilling. Journal of Geophysical Research 104, 10295–10306.

Lin, J., Horwitz, J.L., Wilson, G.R., Ho, C.W., Brown, D.G., 1992. A semikinetic model for early stage plasmaspheric refilling, 2, effects of wave–particle interactions. Journal of Geophysical Research 97, 1121–1134.

Lin, J., Horwitz, J.L., Wilson, G.R., Brown, D.G., 1994. Equatorial heating and hemispheric decoupling effects on inner magnetospheric core plasma evolution. Journal of Geophysical Research 99, 5727–5744.

Olsen, R.C., Scott, L.J., Boardsen, S.A., 1994. Comparison between Liouville's theorem and observed latitudinal distributions of trapped ions in the plasmapause region. Journal of Geophysical Research 99, 2191–2203.

Shkarofsky, I.P., Johnston, T.W., Bachynski, M.P., 1966. The Particle Kinetics of Plasmas. Addison-Wesley, London.

Singh, N., 1988. Refilling of a plasmaspheric flux tube — microscopic plasma processes. In: Moore, T.E., Waite, J.H., Jr. (Eds.), Modeling Magnetospheric Plasma, Geophysical Monograph Series, vol. 44. American Geophysical Union, pp. 87–100.

Singh, N., 1996. Effects of electrostatic ion cyclotron wave instability on plasma flow during early stage plasmaspheric refilling. Journal of Geophysical Research 101, 17217–17227.

Singh, N., 1998. High-altitude trapping of beam ions by self-generated plasma waves in interhemispheric plasma flows. Journal of Geophysical Research 25, 1829–1833.

Singh, N., Horwitz, J.L., 1992. Plasmaspheric refilling: recent observations and modeling. Journal of Geophysical Research 97, 1047–1079.

Singh, N., Wilson, G.R., Horwitz, J.L., 1994. Comparison of hydrodynamic and semikinetic treatments for a plasma flow along closed field lines. Journal of Geophysical Research 99, 11495–11506.

Sojka, J., Schunk, R.W., Johnson, J.F., Waite, J.H., Chappell, C.R., 1983. Characteristics of thermal and superthermal ions associated with the dayside plasma trough as measured by the Dynamics Explorer retarding ion mass spectrometer. Journal of Geophysical Research 88, 7895–7911.